Journal of Organometallic Chemistry, 414 (1991) 227–244
Elsevier Sequoia S.A., Lausanne
JOM 21879

Physical properties of interannular bridged ferrocenophanium salts: structural, NMR, EPR, and Mössbauer studies

Teng-Yuan Dong *, Hsiu-Mei Lin, Ming-Yhu Hwang, Ting-Yu Lee, Li-Hong Tseng
Institute of Chemistry, Academia Sinica, Nankang, Taipei (Taiwan)

Shie-Ming Peng * and Gene-Hsiang Lee
Department of Chemistry, National Taiwan University, Taipei (Taiwan)

(Received February 8th, 1991)

Abstract

The X-ray structure of 1,1′-(propane-1,3-diyl)ferrocenium iodide has been determined at 298 K: monoclinic, $C2/c$, $a = 15.986(3)$, $b = 15.125(3)$, $c = 21.793(3)$ Å, and $\beta = 93.555(11)°$; $Z = 8$, $D_{calcd} = 2.597$ g cm^{-3}, $R_F = 0.044$, and $R_{WF} = 0.050$. The compound 1,1′-(pentane-1,5-diyl)ferrocenium triiodide crystallizes in the triclinic space group $P\bar{1}$ with four molecules in a unit cell with dimensions $a = 9.5435(14)$, $b = 13.1195(22)$, $c = 15.2591(23)$ Å, $\alpha = 106.317(13)$, $\beta = 85.978(12)$, $\gamma = 90.872(13)°$. The final discrepancy factors are $R_F = 0.062$ and $R_{WF} = 0.063$. The physical properties of ferrocenophanium salts are reported. The EPR and Mössbauer results suggest that the electronic ground state of the interannular bridged ferrocenophanium cations is $^2E_{2g}$. The changes of quadrupole splittings, proton chemical shifts, and low-symmetry parameters can be explained in terms of tilting of the Cp ring from parallel geometry.

Introduction

Recent results obtained for the mixed-valence biferrocenium salt **1** clearly indicate that the tilt of the cyclopentadienyl rings has a significant influence on the rate of electron transfer [1]. We have systematically investigated a series of bridged ferrocenium cations **2–7** to further our understanding of the effects of this tilting on the electronic structure of these cations.

Considerable progress has been made in the area of neutral bridged ferrocene derivatives [2–12]. A useful short review has appeared [13] together with a survey of recent developments in this area [14]. When the cyclopentadienyl rings in ferrocene are linked by an interannular bridge, the Cp rings may be displaced from their preferred parallel plane arrangement. Some insight into the effect of this structural change can be obtained through a comparative study of the spectral properties of ferrocenophanes and of analogous ferrocenes. These studies have included the

0022-328X/91/$03.50

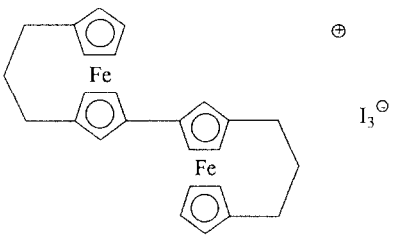

(1)

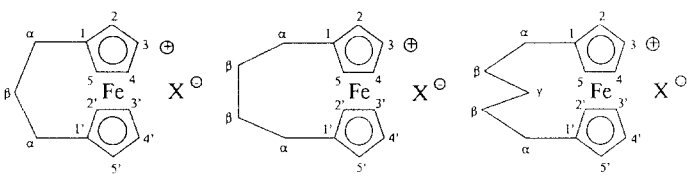

(2) X=I_3
(3) X=PF_6

(4) X=I_3
(5) X=PF_6

(6) X=I_3
(7) X=PF_6

correlation of redox potentials with structure conformational properties [9], and the sensitivity of visible absorption [12] and Mössbauer spectra [6,7] to the presence of an interannular bridge. An analysis of polarographic half-wave potentials has shown correlations between the potentials and the iron–ring distances [9]. There is a linear relationship between change in iron–ring distances and change of Mössbauer parameters. Relatively few investigations have been carried out on bridged ferrocenophanium cations. ^{57}Fe Mössbauer spectra of **2** and **4** were reported by Sano [3]. In this paper the EPR, NMR, and Mössbauer data for ferrocenophanium cations **2**–**7** are analyzed in terms of structural characteristics.

Experimental

Compound preparation

Samples of 1,1′-(propane-1,3-diyl)ferrocene [15], 1,1′-(butane-1,4-diyl)ferrocene [16], and 1,1′-(pentane-1,5-diyl)ferrocene [17] were prepared according to literature methods and identified by melting point, ^{1}H NMR, and mass spectral data.

Samples of **2**, **4**, and **6** were prepared by oxidizing the neutral ferrocenophanes in 1 : 1 benzene–hexane solution with stoichiometric amounts of I_2 in benzene. The PF_6 salts **3**, **5**, and **7** were made by oxidizing neutral ferrocenophanes in diethyl ether solution by dropwise addition of a diethyl ether solution containing a stoichiometric amount of *p*-benzoquinone and HPF_6. The dark microcrystals were collected by filtration and washed first with benzene and then with diethyl ether. Anal. **2**: Found: C, 22.58; H, 2.13. $C_{13}H_{14}FeI_{11/3}$ calcd.: C, 22.58; H, 2.04%. **3**: Found: C, 42.10; H, 3.92. $C_{13}H_{14}FePF_6$ calcd.: C, 42.08; H, 3.80%. **4**: Found: C, 26.71, H, 2.72. $C_{14}H_{16}FeI_3$ calcd.: C, 27.08; H, 2.60%. **5**: Found: C, 43.35; H, 4.23. $C_{14}H_{16}FePF_6$ calcd.: C, 43.67; H, 4.19%. **6**: Found: C, 28.35; H, 2.78. $C_{15}H_{18}FeI_3$ calcd.: C, 28.38; H, 2.86%. Found: C, 44.52; H, 4.28. $C_{15}H_{18}FePF_6$ calcd.: C, 45.14; H, 4.55%.

Physical methods

^{57}Fe Mössbauer measurements were made at the Academia Sinica on a constant-acceleration-type instrument. The source, which consisted of ~ 35 mCi of ^{57}Co diffused into a 12 μm rhodium matrix, was connected to a Ranger Scientific Model VT-900 velocity transducer. An Ortec Model 5600 multichannel analyzer, scanned over 1024 channels, received the logic pulses from the single-channel analyzer. Computer fitting of the ^{57}Fe Mössbauer data to Lorentzian lines were performed by a modified version of a program previously reported [18]. Velocity calibrations were made with a 99.99% pure 10 μm iron foil. Typical line widths for all three pairs of iron lines fell in the range of 0.25–0.28 mm/s. Isomer shifts are reported with respect to iron foil at 300 K.

^{1}H NMR spectra were run on a Bruker MSL 200 spectrometer. Mass spectra were obtained with a VG system, Model 70-250S. Electron paramagnetic resonance data (X band) were collected with a Bruker ER200D-SRC spectrometer. The magnetic field was calibrated with a Bruker NMR Gauss meter ER035M. DPPH was used to gauge the microwave frequency. A direct-immersion dewar, which was inserted into the cavity, was used to obtain 77 K data.

Structural determination of **2**

A block crystal (0.29 × 0.07 × 0.11 mm), which was grown by slowly diffusing the hexane solution into a CH_2Cl_2 solution of **2**, was used for data collected at room temperature. Cell dimensions and space group data were determined by standard methods on an Enraf Nonius CAD4 diffractometer. The θ–2θ scan technique was used to record the intensities for all nonequivalent reflects for which $1 < 2\theta < 44.8°$. Absorption corrections were made. Of the 3425 independent intensities, there were 1959 with $F_o > 2.5\ \sigma(F_o^2)$, where $\sigma(F_o^2)$ was estimated from counting statistics. These data were used in the final refinement of the structural parameters. The X-ray crystal data are summarized in Table 1.

A three-dimensional Patterson synthesis was used to determine heavy-atom positions, which phased the data sufficiently well to permit location of the remaining non-hydrogen atoms by Fourier synthesis. All nonhydrogen atoms were refined anisotropically. During the final cycles of refinement fixed hydrogen contributions with C–H bond lengths fixed at 1.08 Å were applied. The final positional parameters for all atoms can be found in Table 2, and selected bond distances and angles are given in Table 3. Listings of the thermal parameters and observed and calculated structure factors are available from the authors as supplementary material.

Structural determination of **6**

A block crystal (0.44 × 0.13 × 0.22 mm) was obtained following the same manner for **2**. Of the 4770 independent intensities, there were 3349 with $F_o > 2.5\sigma(F_o^2)$. These data were used in the final refinement of structural parameters. Details of data collection and unit cell parameters are given in Table 1.

Structure refinement was carried out in the same manner as described for **2**. The greatest residual electron density upon completion of refinement was in the vicinity of iodide moieties. Atomic coordinates are given in Table 4. Listings of the thermal parameters and observed and calculated structure factors are available as supplementary material.

Results

Molecular structure of **2**

The results of our crystallographic study of **2** show that it crystallizes in the monoclinic space group $C2/c$. There are two crystallographically independent molecules in the unit cell, and the molecular structures and atomic labelling schemes for cations and the polyiodide chain are shown in Figs. 1 and 2, respectively. The cation associated with an I_5^- anion lies on a crystallographic mirror plane and is located about a twofold axis. As shown in Fig. 3, the packing arrangement in **2** consists of planar layers of cations and polyiodide anion chains. The trimethylene bridges are disordered whereby the C7A and C7B atoms may exist in two equivalent sites generated by the twofold axis. Atomic coordinates and important parameters are given in table 2 and 3, respectively.

Molecular structure of **6**

Compound **6** crystallizes in the triclinic space group $P\bar{1}$. There are two crystallographically independent molecules in the unit cell. Figure 4 shows the molecular structures and atomic labelling schemes for cations and triiodide anions. The pentamethylene bridge associated with Fe_B is disordered whereby the C8B atom may exists in two equivalent sites. Atomic coordinates and selected bond distances and angles are shown in Table 4 and 5, respectively.

Nuclear magnetic resonance

As shown in Fig. 5, the ^1H NMR spectra were obtained from deoxygenated CD_2Cl_2 solutions. The experimental shifts for the molecules of interest will be

Table 1

Experimental and crystal data for the X-ray structures of **2** and **6**

Compound	**2**	**6**
Formula	$C_{19.5}H_{21}Fe_{1.5}I_{5.5}$	$C_{15}H_{16}FeI_3$
Crystal system	monoclinic	triclinic
Space group	$C2/c$	$P\bar{1}$
a (Å)	15.986(3)	9.5435(14)
b (Å)	15.125(3)	13.1195(22)
c (Å)	21.793(3)	15.2591(23)
α (deg)		106.317(13)
β (deg)	93.555(11)	85.978(12)
γ (deg)		90.872(13)
V (Å^3)	5259.2(16)	1829.0(5)
Z	8	4
Formula weight (g mol^{-1})	1028.04	629.82
ρ_{calcd} (g cm^{-3})	2.597	2.287
μ (mm^{-1})	7.24	5.83
λ (Å)	0.70930	0.70930
2θ (max)	44.8	44.9
Trans. coeff. (max, min)	0.9985, 0.8142	0.9999, 0.7856
R_F	0.044	0.062
R_{WF}	0.050	0.063

Table 2

Atomic coordinates and thermal parameters for **2**

	x	*y*	*z*	B_{iso} [a]
I1	0	0.17037(16)	1/4	5.96(13)
I2	−0.16002(11)	0.15703(11)	0.33233(8)	5.49(8)
I3	−0.29632(11)	0.15481(12)	0.40707(8)	6.01(9)
I4	−0.48557(12)	0.17333(13)	0.49004(9)	6.56(10)
I5	−0.63180(10)	0.17002(11)	0.56747(7)	4.66(8)
I6	−0.77603(11)	0.16890(13)	0.64109(8)	6.08(10)
FeA	0.81803(19)	0.01502(20)	0.06683(14)	3.71(15)
C1A	0.7312(13)	−0.0700(14)	0.0986(10)	4.8(12)
C2A	0.6883(12)	0.0005(16)	0.0673(10)	5.1(13)
C3A	0.7102(13)	0.0785(14)	0.0950(9)	4.1(11)
C4A	0.7673(13)	0.0601(15)	0.1447(9)	4.1(11)
C5A	0.7815(14)	−0.0355(15)	0.1494(9)	5.2(12)
C6A	0.8408(18)	−0.0816(17)	0.1925(11)	7.2(15)
C7A [b]	0.922(3)	−0.072(3)	0.1943(20)	5.2(24)
C7A′	0.914(3)	−0.126(3)	0.1661(20)	4.8(23)
C8A	0.9707(17)	−0.0788(17)	0.1375(11)	7.0(15)
C9A	0.9425(14)	−0.0305(17)	0.0813(11)	6.1(13)
C10A	0.9372(13)	0.0659(15)	0.0712(10)	4.4(12)
C11A	0.8978(14)	0.0851(13)	0.0126(10)	4.5(11)
C12A	0.8730(13)	0.0053(16)	−0.0169(10)	4.8(11)
C13A	0.9015(13)	−0.0650(13)	0.0230(11)	4.8(12)
FeB	0	0.4613(3)	1/4	3.71(21)
C1B	0.0340(13)	0.4960(15)	0.1636(9)	4.6(12)
C2B	0.0601(13)	0.4075(13)	0.1760(10)	4.1(11)
C3B	0.1148(13)	0.4100(13)	0.2295(9)	4.3(11)
C4B	0.1244(14)	0.4962(15)	0.2498(10)	5.2(12)
C5B	0.0720(14)	0.5557(14)	0.2088(10)	5.1(12)
C6B	0.0597(20)	0.6530(15)	0.2176(14)	8.9(18)
C7B [b]	−0.013(5)	0.686(3)	0.2301(23)	7.4(39)

[a] B_{iso} is the mean of the principal axes of the thermal ellipsoid. [b] Occupancy of C7A and C7B = 0.5.

found in Table 6. Shifts were taken relative to the TMS peak. The isotropic shifts were calculated relative to the shifts for the corresponding ferrocenophanes.

Electron paramagnetic resonance

X band EPR spectra were run at 300 and 77 K for samples **2**–**7**. Axial-type spectra were observed for 1,1′-(propane-1,3,-diyl)-, 1,1′-(butane-1,4-diyl)-, and 1,1′-(pentane-1,5-diyl)ferrocenium cations in H_2SO_4 frozen solutions. The *g* values extracted from all of these spectra are collected in Table 7, together with some *g* values from the literature.

^{57}Fe Mössbauer characteristics

As shown in Fig. 6, the Mössbauer spectra were run at 300 K for compounds **2**–**7**. The absorption peaks in each spectrum were fitted by least-squares to Lorentzian lines and the resulting fitting parameters are summarized in Table 8.

Discussion

Structural description of 2

A shown in Fig. 1, the Cp rings are nearly eclipsed, and the Fe–C distances range

Table 3

Selected bond distances (Å) and angles (deg) for **2**

Distance			
I(1)–(2)	3.2207(5)	C(1A)–C(5A)	1.4262(2)
I(2)–I(3)	2.8003(4)	C(2A)–C(3A)	1.3611(2)
I(4)–I(5)	2.9671(5)	C(3A)–C(4A)	1.4004(2)
I(5)–I(6)	2.8895(5)	C(4A)–C(5A)	1.4663(3)
Fe(A)–C(1A)	2.0442(3)	C(5A)–C(6A)	1.4686(2)
Fe(A)–C(2A)	2.0861(4)	C(6A)–C(7A)	1.3043(2)
Fe(A)–C(3A)	2.0979(3)	C(7A)–C(8A)	1.5061(2)
Fe(A)–C(4A)	2.0428(3)	C(8A)–C(9A)	1.4726(2)
Fe(A)–C(5A)	2.0720(2)	C(9A)–C(10A)	1.4762(3)
Fe(A)–C(9A)	2.1107(4)	C(9A)–C(13A)	1.4876(2)
Fe(A)–C(10A)	2.0513(3)	C(10A)–C(11A)	1.4185(2)
Fe(A)–C(11A)	2.0817(3)	C(11A)–C(12A)	1.4127(2)
Fe(A)–C(12A)	2.0790(3)	C(12A)–C(13A)	1.4301(2)
Fe(A)–C(13A)	2.0774(3)	C(1B)–C(2B)	1.4230(3)
Fe(B)–C(1B)	2.0599(3)	C(1B)–C(5B)	1.4424(2)
Fe(B)–C(2B)	2.0924(3)	C(2B)–C(3B)	1.4139(2)
Fe(B)–C(3B)	2.0667(3)	C(3B)–C(4B)	1.3823(2)
Fe(B)–C(4B)	2.0578(4)	C(4B)–C(5B)	1.4890(2)
Fe(B)–C(5B)	2.0731(3)	C(5B)–C(6B)	1.4986(3)
C(1A)–C(2A)	1.4194(2)	C(6B)–C(7B)	1.3089(2)
Angles			
I(2)–I(1)–I(2)	172.8	C(10A)–C(9A)–C(13A)	101.592(7)
I(1)–I(2)–I(3)	176.7	C(9A)–C(10A)–C(11A)	110.8
I(4)–I(5)–I(6)	178.9	C(10A)–C(11A)–C(12A)	109.342(9)
C(2A)–C(1A)–C(5A)	109.30(1)	C(11A)–C(12A)–C(12A)	106.78(1)
C(1A)–C(2A)–C(3A)	109.55(1)	C(9A)–C(13A)–C(12A)	111.43(1)
C(2A)–C(3A)–C(4A)	107.949(9)	C(2B)–C(1B)–C(5B)	110.68(1)
C(3A)–C(4A)–C(5A)	109.9	C(1B)–C(2B)–C(3B)	106.9
C(1A)–C(5A)–C(4A)	103.249(7)	C(2B)–C(3B)–C(4B)	109.9
C(1A)–C(5A)–C(6A)	129.29(1)	C(3B)–C(4B)–C(5B)	109.32(1)
C(4A)–C(5A)–C(6A)	127.1	C(1B)–C(5B)–C(4B)	103.23(1)
C(6A)–C(7A)–C(8A)	122.13(1)	C(1B)–C(5B)–C(6B)	130.474(7)
C(7A)–C(8A)–C(9A)	120.166(9)	C(4B)–C(5B)–C(6B)	126.165(7)
C(8A)–C(9A)–C(10A)	128.7	C(5B)–C(6B)–C(7B)	121.8
C(8A)–C(9A)–C(13A)	129.22(1)		

from 2.03 to 2.15 Å. The spread of distances is due to the nonparallel Cp rings where the angles between the two least-squares rings of $Fe_A(Cp)_2$ and $Fe_B(Cp)_2$ are 13.6 and 12.9°, respectively. The average of these Fe–C distances, i.e., 2.073 Å, is larger than 2.045 Å observed for ferrocene [19] and it is closer to the value of 2.07 Å found for ferrocenium [20]. Furthermore, the distance between Fe and the centre of mass of the ring in each cation is 1.66 Å which is shorter than the value of 1.70 Å observed for the ferrocenium cation [20]. The average distance of Fe to Cp ring is 1.673 Å which lies midway between the 1.658 Å observed for 1,1′-(propane-1,3-diyl)ferrocenium $(TCNQ)_2$ [4] and 1.70 Å observed for ferrocenium cation [20]. A direct comparison is made between **2** and related molecules (see Table 9). From this comparison, we can conclude that there is an increased metal–ring overlap in **2** as the interannular trimethylene bridge squeezes the Fe atom. This is also consistent with our EPR studies.

Table 4

Atomic coordinates and thermal parameters for **6**

	x	*y*	*z*	B_{iso} [a]
I1	0.83369(20)	0.60363(15)	0.13594(12)	6.70(10)
I2	0.71479(17)	0.39729(13)	0.03954(11)	5.72(9)
I3	0.60296(20)	0.19282(14)	−0.05786(14)	7.20(11)
I4	0.40869(21)	0.92386(14)	0.79249(14)	7.41(11)
I5	0.32506(17)	0.71400(13)	0.68903(11)	5.32(8)
I6	0.23169(21)	0.50487(14)	0.58291(12)	6.84(11)
FeA	0.4418(3)	0.71636(23)	0.33714(24)	5.05(17)
C1A	0.285(3)	0.6504(17)	0.2444(18)	7.2(15)
C2A	0.420(3)	0.6104(17)	0.2119(18)	7.0(16)
C3A	0.4715(24)	0.5606(18)	0.2760(16)	6.1(15)
C4A	0.375(3)	0.5752(18)	0.3505(16)	6.3(14)
C5A	0.252(3)	0.6324(20)	0.3352(23)	11.9(21)
C6A	0.125(3)	0.6590(21)	0.3915(24)	12.1(22)
C7A	0.042(3)	0.754(3)	0.3871(23)	12.8(24)
C8A	0.112(3)	0.8535(20)	0.4008(23)	10.2(21)
C9A	0.179(4)	0.903(3)	0.481(3)	20.1(35)
C10A	0.315(4)	0.9136(22)	0.499(3)	16.1(27)
C11A	0.4374(24)	0.8633(17)	0.4424(19)	8.8(15)
C12A	0.461(3)	0.8829(16)	0.3585(18)	7.4(15)
C13A	0.585(3)	0.8307(17)	0.3205(17)	6.6(15)
C14A	0.6293(24)	0.7730(19)	0.3848(19)	7.6(17)
C15A	0.531(3)	0.7975(21)	0.4598(16)	7.5(17)
FeB	0.1492(3)	0.24575(22)	0.11292(10)	4.01(15)
C1B	0.309(3)	0.3233(17)	0.1896(17)	7.7(17)
C2B	0.2861(24)	0.3672(16)	0.1181(18)	7.0(14)
C3B	0.1458(24)	0.4089(15)	0.1337(15)	5.2(12)
C4B	0.1018(25)	0.3912(17)	0.2173(15)	6.3(13)
C5B	0.201(3)	0.3409(20)	0.2534(18)	8.7(18)
C6B	0.201(5)	0.308(3)	0.3383(18)	17.4(35)
C7B	0.149(4)	0.227(3)	0.3595(21)	14.8(31)
C8B	0.203(5)	0.127(4)	0.287(4)	7.3(31)
C8B′	0.032(5)	0.173(3)	0.305(4)	9.4(33)
C9B	0.081(5)	0.0895(22)	0.2705(18)	13.6(29)
C10B	0.054(3)	0.0265(22)	0.1723(20)	9.7(9)
C11B	0.077(3)	0.0857(17)	0.0996(14)	5.8(13)
C12B	0.1980(23)	0.0856(18)	0.0456(14)	5.6(13)
C13B	0.1723(21)	0.1475(17)	−0.0110(14)	5.4(13)
C14B	0.033(3)	0.1885(17)	0.0077(14)	5.6(13)
C15B	−0.0254(24)	0.1528(19)	0.0775(15)	6.1(14)

[a] B_{iso} is the mean of the principal axes of the thermal ellipsoid.

As viewed down the *a* axis (Fig. 3), the solid-state structure of **2** is composed of parallel sheets of cations and linear polyiodide chains in unit of I_3–I_5–I_3. The two I_3^- ions are asymmetric but are disposed equally relative to the I_5^- ion. There is a slight I_2–I^- character, where I(4)–I(5) = 2.967(15) and I(5)–I(6) = 2.8895(5) Å. The average distance of I–I in I_3^- is 2.9283(5) Å which is in accord with the standard value of 2.920 Å proposed for the centrosymmetric I_3^- ion [21]. The centrosymmetric I_5^- ion is of I_2–I^-–I_2 character, where I(1)–I(2) = 3.2207(5) Å and I(2)–I(3) = 2.8003(4) Å. The I–I bond length in the I_2 units, 2.8003 Å, is significantly greater

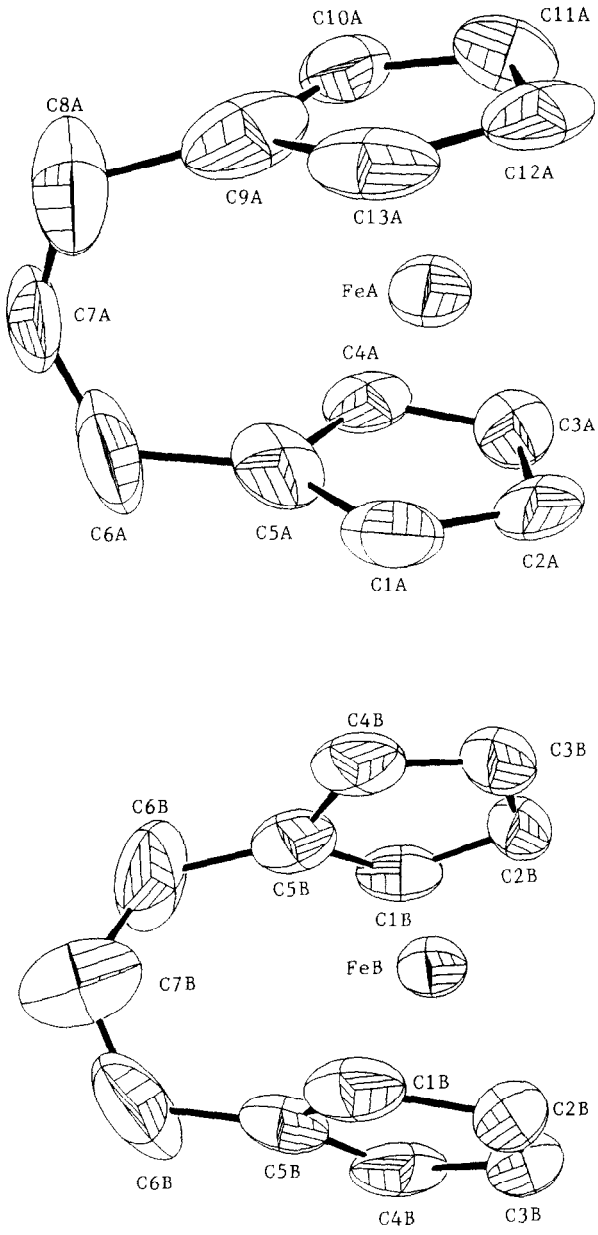

Fig. 1. ORTEP plot of two crystallographically independent cations of **2**.

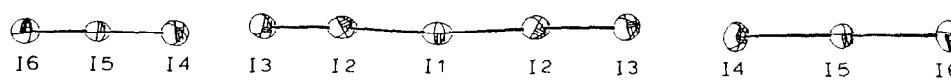

Fig. 2. ORTEP plot of the polyiodide anion of **2**.

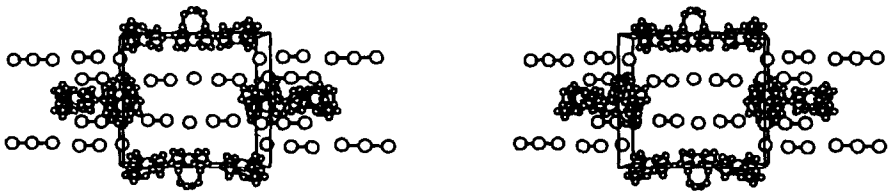

Fig. 3. Stereoview of **2** as viewed down the *a* axis.

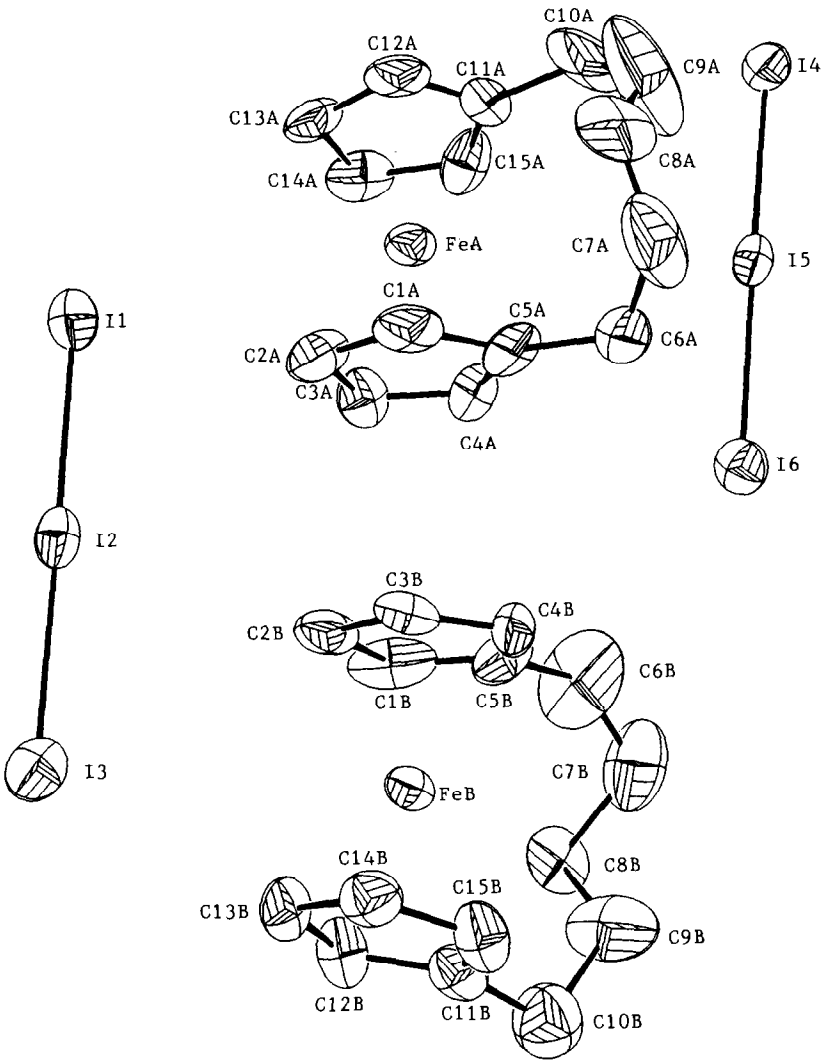

Fig. 4. ORTEP plot of two independent molecules of **6**.

Table 5

Selected bond distances (Å) and angles (deg) for **6**

Distances			
I(1)–I(2)	2.9467(5)	C(5A)–C(6A)	1.4238(2)
I(2)–I(3)	2.9050(5)	C(6A)–C(7A)	1.5066(2)
I(4)–I(5)	2.8944(5)	C(7A)–C(8A)	1.4261(2)
I(5)–I(6)	2.9284(5)	C(8A)–C(9A)	1.4067(2)
Fe(A)–C(1A)	2.1355(4)	C(9A)–C(10A)	1.3425(2)
Fe(A)–C(2A)	2.045(4)	C(10A)–C(11A)	1.4518(3)
Fe(A)–C(3A)	2.0089(4)	C(11A)–C(12A)	1.3779(2)
Fe(A)–C(4A)	2.0089(3)	C(11A)–C(15A)	1.3413(2)
Fe(A)–C(5A)	2.1033(3)	C(12A)–C(13A)	1.3824(2)
Fe(A)–C(11A)	2.1333(4)	C(13A)–C(14A)	1.4832(2)
Fe(A)–C(12A)	2.1236(4)	C(14A)–C(15A)	1.3946(2)
Fe(A)–C(13A)	2.0701(3)	C(1B)–C(2B)	1.4001(2)
Fe(A)–C(14A)	2.0301(3)	C(1B)–C(5B)	1.3430(2)
Fe(A)–C(15A)	2.1065(4)	C(2B)–C(3B)	1.4329(2)
Fe(B)–C(1B)	2.0650(3)	C(3B)–C(4B)	1.3950(2)
Fe(B)–C(2B)	2.0328(3)	C(4B)–C(5B)	1.3898(2)
Fe(B)–C(3B)	2.0742(4)	C(5B)–C(6B)	1.4761(2)
Fe(B)–C(4B)	2.1448(3)	C(6B)–C(7B)	1.2786(2)
Fe(B)–C(5B)	2.2400(3)	C(7B)–C(8B)	1.5283(3)
Fe(B)–C(11B)	2.1589(4)	C(8B)–C(9B)	1.2709(2)
Fe(B)–C(12B)	2.1063(4)	C(9B)–C(10B)	1.5319(3)
Fe(B)–C(13B)	1.9663(4)	C(10B)–C(11B)	1.5254(2)
Fe(B)–C(14B)	1.9795(3)	C(11B)–C(12B)	1.3706(2)
Fe(B)–C(15B)	2.0615(3)	C(11B)–C(15B)	1.4432(2)
C(1A)–C(2A)	1.4021(2)	C(12B)–C(13B)	1.3768(2)
C(1A)–C(5A)	1.4816(2)	C(13B)–C(14B)	1.4214(2)
C(2A)–C(3A)	1.4358(2)	C(14B)–C(15B)	1.3614(2)
C(3A)–C(4A)	1.3832(2)	COM–COM [a]	3.3669(6)
C(4A)–C(5A)	1.4694(2)		
Angles			
I(1)–I(2)–I(3)	178.8	C(11A)–C(15A)–C(14A)	106.16(1)
I(4)–I(5)–I(6)	178.0	C(2B)–C(1B)–C(5B)	112.41(1)
C(2A)–C(1A)–C(5A)	108.50(1)	C(1B)–C(2B)–C(3B)	107.09(1)
C(1A)–C(2A)–C(3A)	108.30(1)	C(2B)–C(3B)–C(4B)	102.43(1)
C(2A)–C(3A)–C(4A)	109.28(1)	C(3B)–C(4B)–C(5B)	114.32(1)
C(3A)–C(4A)–C(5A)	109.18(1)	C(1B)–C(5B)–C(4B)	103.51(1)
C(1A)–C(5A)–C(4A)	104.58(1)	C(1B)–C(5B)–C(6B)	123.54(1)
C(1A)–C(5A)–C(6A)	127.06(1)	C(4B)–C(5B)–C(6B)	132.95(1)
C(4A)–C(5A)–C(6A)	128.24(1)	C(5B)–C(6B)–C(7B)	131.70(1)
C(5A)–C(6A)–C(7A)	118.64(1)	C(6B)–C(7B)–C(8B)	108.44(1)
C(6A)–C(7A)–C(8A)	118.45(1)	C(7B)–C(8B)–C(9B)	94.14(1)
C(7A)–C(8A)–C(9A)	122.95(1)	C(8B)–C(9B)–C(10B)	118.49(1)
C(8A)–C(9A)–C(10A)	132.18(1)	C(9B)–C(10B)–C(11B)	116.32(1)
C(9A)–C(10A)–C(11A)	128.99(1)	C(10B)–C(11B)–C(12B)	126.03(1)
C(10A)–C(11A)–C(12A)	116.84(1)	C(10B)–C(11B)–C(15B)	125.25(1)
C(10A)–C(11A)–C(15A)	116.84(1)	C(12B)–C(11B)–C(15B)	108.71(1)
C(12A)–C(11A)–C(15A)	114.52(1)	C(11B)–C(12B)–C(13B)	106.79(1)
C(11A)–C(12A)–C(13A)	105.55(1)	C(12B)–C(13B)–C(14B)	110.21(1)
C(12A)–C(13A)–C(14A)	106.94(1)	C(13B)–C(14B)–C(15B)	106.64(1)
C(13A)–C(14A)–C(15A)	106.70(1)	C(11B)–C(15B)–C(14B)	107.60(1)

[a] COM: Centre of mass of Cp ring.

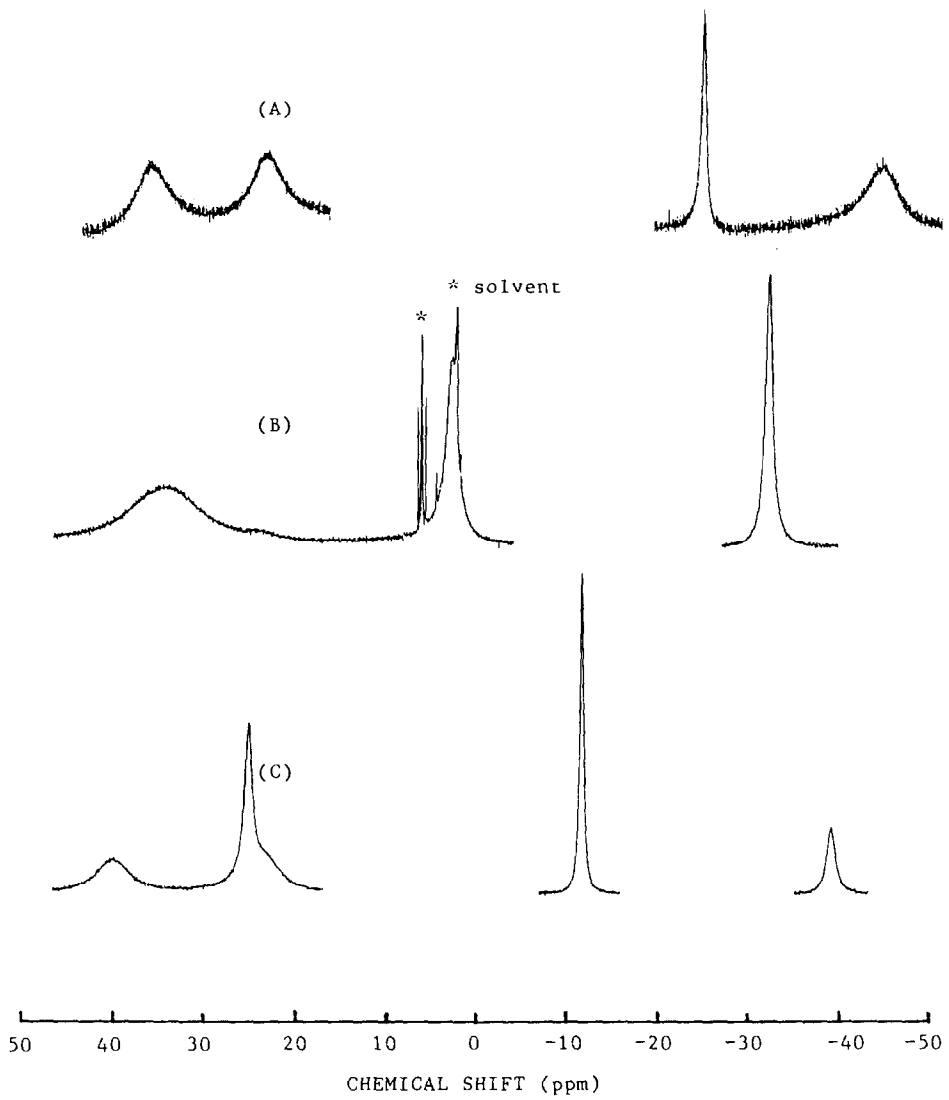

Fig. 5. ^{1}HNMR spectra of **2** (A), **4** (B), and **6** (C) in CD_2Cl_2.

than the value of 2.68 Å found in crystalline I_2 [22]. All polyiodide chains are translationally equivalent, with only Van der Waals interactions between them.

Structure description of ***6***

Drawings of the two independent molecules are given in Fig. 4. A comparison is also made between **2** and **6** (see Table 9). The two Cp rings in each ferrocenium cation are nearly eclipsed. From the spread of Fe–C distances, we can conclude that the two Cp rings are not parallel as found in the ferrocenium cation [20]. In this case, the long interannular pentamethylene bridge opens the Cp rings from the parallel geometry, and the angles between the two least-squares Cp rings in $Fe_A(Cp)_2$ and $Fe_B(Cp)_2$ are 8.2 and 13.4°, respectively. As shown in Fig. 7, ring

Table 6

^{1}H NMR data for paramagnetic ferrocenophanium cations in CD_2Cl_2

Compound	Chemical shifts [a] (ppm)	$\Delta\delta$ [b] (ppm)
$(C_5H_5)_2FeI_3$ [c]	31.9 (10H, Cp)	27.86
2 [d]	36.44 (4H, Cp)	32.42
	23.00 (4H, Cp)	19.03
	−26.64 (2H, β-CH_2)	−25.58
	−46.80 (4H, α-CH_2)	−48.74
4 [e]	34.00 (8H, Cp)	29.97
	2.00 (4H, β-CH_2)	0.18
	−34.32 (4H, α-CH_2)	−36.73
6 [f]	39.77 (4H, Cp)	35.71
	24.85 (4H, β-CH_2)	23.06
	~ 24.0 (4H, Cp)	~ 20.05
	−12.72 (4H, α-CH_2)	−15.04
	−40.46 (2H, γ-CH_2)	−42.43

[a] Shifts were taken relative to the TMS peak. [b] Isotropic shifts were calculated relative to the shift for the corresponding diamagnetic ferrocenophanes. [c] ^{1}H NMR of ferrocene (CD_2Cl_2): δ 4.04. [d] ^{1}H NMR of 1,1′-(propane-1,3-diyl)ferrocene ($CDCl_3$): 4.02 (s, 2H, Cp); 3.97 (s, 2H, Cp); 1.94 (s, 6H, $(CH_2)_3$). [e] ^{1}H NMR of 1,1′-(butane-1,4-diyl)ferrocene ($CDCl_3$): 4.05 (s, 4H, Cp); 4.02 (s, 4H, Cp); 2.41 (m, 4H, α-CH_2); 1.82 (m, 4H, β-CH_2). [f] ^{1}H NMR of 1,1′-(pentane-1,5-diyl)ferrocene ($CDCl_3$): 4.06 (t, 4H, Cp); 3.95 (t, 4H, Cp); 2.32 (t, 4H, α-CH_2); 1.97 (m, 2H, γ-CH_2); 1.79 (m, 4H, β-CH_2).

tilting can be described in various ways. Ballhausen and Dahl [23] have discussed the effect of ring tilting of the kind depicted in Fig. 7a. In this structure, there is no change in Fe–C and Fe–ring distances as the rings tilt. Although we use the model as shown in Fig. 7a to explain qualitatively the physical properties of **2** and **6**, the best molecular descriptions for **2** and **6** are those in Figs. 7b and 7c, respectively.

The average value of I–I in two asymmetric I_3^- is 2.9186(5) Å which agrees well with the value of 2.920 Å for symmetric I_3^- [21].

Table 7

EPR data for ferrocenium cations

Compound	T (K)	$g_\parallel$	$g_\perp$	k	x	ζ [a]	δ [a]
ferrocenium [b,f]	12	4.35	1.26	0.76	1.23	300	270
1,1′-dimethyl-ferrocenium I_3 [c]	12	3.67	1.77				
2	77	~ 2.00 [d]					
3	300	2.00 (490) [e]					
	77	2.00 (560) [e]					
4	77	no signal					
5	300	2.22	2.01				
	77	2.20	2.03				
7	77	3.35	1.96				
2 [f]	77	3.75	1.66	0.784	0.672	310	460
4 [f]	77	3.72	1.71	0.829	0.607	330	540
6 [f]	77	3.35	1.87	0.952	0.379	380	1000

[a] In cm^{-1}. [b] From ref. 31. [c] From ref. 32. [d] The half-height linewidth is ~1500 gauss. [e] The half-height linewidths in gauss are given in parentheses. [f] In H_2SO_4 frozen solution.

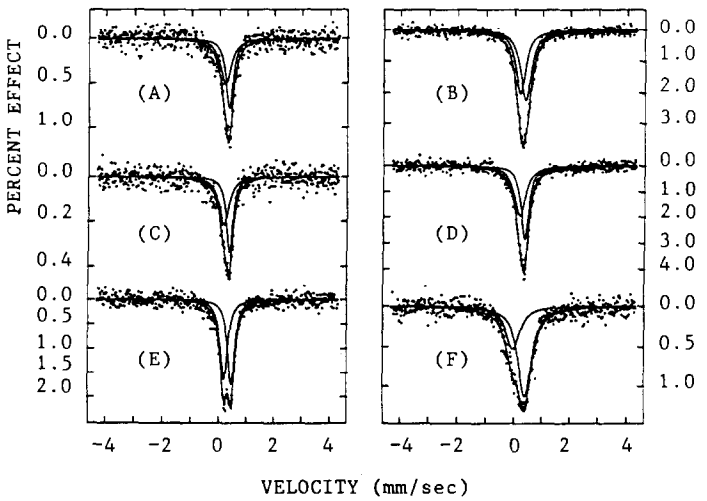

Fig. 6. ^{57}Fe Mössbauer spectra of **2** (A), **3** (B), **4** (C), **5** (D), **6** (E), and 7 (F).

Table 8

^{57}Fe Mössbauer least-squares fitting parameters at 300 K

Compound	ΔE_Q (mm/s)	δ (mm/s)	Γ [a] (mm/s)
2	0.1484	0.3825	0.4721, 0.3140
3	0.1925	0.4019	0.4470, 0.4613
4	0.2074	0.3793	0.4280, 0.2770
5	0.1885	0.3906	0.4828, 0.3298
6	0.2647	0.4342	0.3217, 0.3032
7	0.3879	0.3472	0.7135, 0.5091

[a] Full width at half-height taken from the least-squares fitting program. The width for the line at more negative velocity is listed first for each doublet.

Table 9

Comparison of the important parameters for **2** and **6** with ferrocenium cations

Compound	$Fc(TCNQ)_2$ [a]	**2** [b]	**6** [b]
Fe–C_{ave} (Å)	2.0668(3)	2.0686(3), 2.0800(3)	2.0603(3), 2.0927(4)
		2.0700(3)	2.1114(3), 2.0545(4)
Fe–COM (Å) [c]	1.66, 1.66	1.64, 1.73	
	1.66	1.75, 1.67	
COM–COM (Å) [c]	3.31	3.37	
	3.32	3.38	
Fe–ring (Å)	1.658	1.67, 1.67	1.64, 1.72
		1.68	1.66, 1.73
COM–Fe–COM (deg)		171.2	178.9
		170.9	178.0
tilt angle (deg)	13.8	13.6	8.2
		12.9	13.4

[a] Fc (TCNQ) is 1,1′-(propane-1,3-diyl)ferrocenium $(TCNQ)_2$. From ref. 6. [b] There are two independent molecules in the unit cell and the value associated with Fe(A) is listed first. [c] COM is the centre of mass of the Cp ring.

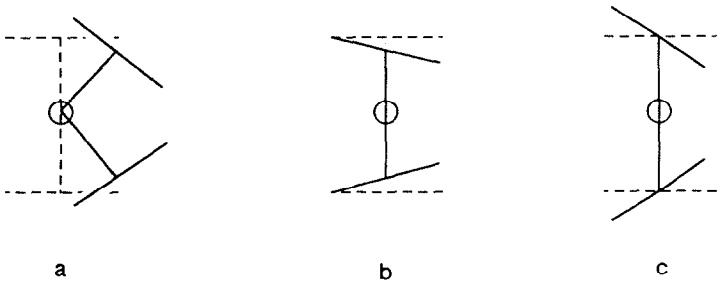

Fig. 7. Various ways of rings tilting in ferrocenium cations. The dashed horizontal lines represent the Cp rings and the central circle is the iron atom.

Theoretical considerations

Using a MO approach to the bonding in metallocenes and related molecules, Ballhausen and Dahl [23] have discussed the effect of ring tilting and have concluded that considerable splaying of the rings (up to 45°) about the metal atom can occur without significant loss of the strength of the metal–ring bonds. The electronic ground state of ferrocene is a singlet, $^1A_{1g}$ ($e_{2g}^4 a_{1g}^2$), where the one-electron molecular orbitals are predominantly d orbital in character: a_{1g} (d_{z^2}) and e_{2g} (d_{xy}, $d_{x^2-y^2}$). Lauher and Hoffmann [24] have derived the fragment orbitals for a bent $(Cp)_2M$ unit from the parallel geometry. Bending back the Cp rings splits the e_{2g} set into orbitals of a_1 ($d_{x^2-y^2}$) and b_2 (d_{xy}) symmetry. The a_{1g} orbitals rise rapidly in energy as the Cp rings are bent back. In such a situation, some metal $d_{x^2-y^2}$ character from a_1 becomes mixes into the a_{1b} orbitals so that the torus of z^2 becomes hybridized away from the Cp rings.

In the case of the ferrocenium cation, the electronic ground state is a doublet, $^2E_{2g}$ ($a_{1g}^2 e_{2g}^3$), as indicated by magnetic susceptibility [25], EPR [26–29], and Mössbauer measurements [3]. In the case of 1,1′-(propane-1,3-diyl)ferrocenium cation, it has also been reported [30] that there is an increased metal–ring overlap as the rings tilt. Under this circumstance the iron ions lose some degree of their Fe^{III} character, and this results in a change of ^{57}Fe Mössbauer parameters. Furthermore, the splitting of e_{2g} orbitals could lead to a slower electronic relaxation time, and this could have a pronounced influence on EPR signals. Here, analyses of Mössbauer and EPR results will be based on these theoretical considerations.

Nuclear magnetic resonance

It is now widely recognized that the study of nuclear resonance in paramagnetic complexes can yield detailed information concerning metal–ligand bonding and electron delocalization. It is of value to apply the NMR technique to elucidate the nature of electron delocalization in the ferrocenophanium cation series.

A comparison of the negative spin density at cyclopentadienyl protons and the positive spin density at α-CH_2 protons leads to the conclusion that the unpaired electron density is delocalized in π-type orbitals, as found in ferrocenium salts and 1,1′-dimethylferrocenium ions [31]. Electron delocalization in ligand σ orbitals has been observed for decamethylferrocenium salts [32], 1,1′-dimethylchromocene [33], and nickel complexes of pyridine [34] and aliphatic amines [35]. The general pattern

of the spin delocalization for metallocene depends on the superposition of the π and σ mechanisms.

It should be pointed out that shifts of cyclopentadienyl protons indicate the degree of delocalization of unpaired electrons. The difference of shifts in each compound does not originate in a difference in electronic effect of interannular bridges. The electronegativity difference between propane-1,3-diyl and pentane-1,5-diyl bridges is probably non existent. In fact, both ferrocenium triiodide and 1,1′-dimethylferrocenium cations have a broad peak assigned as cyclopentadienyl protons at ~ 30 ppm [33]. However, the Cp protons in compounds **2** and **6** split into two sets. The difference in pattern of Cp protons between ferrocenium and **2** can be explained by their different structural characteristics. When the Cp rings tilt away from parallel, geometry, the Fe–C distances are no longer the same and neither is the degree of delocalization of the unpaired electron. If our suggestion is correct, then the Cp protons at 36.4 ppm in **2** can be assigned to $C_{2,5,2',5'}$–H and the other one at 23 ppm can be attributed to $C_{3,4,3',4'}$–H. This assignment is based on the single crystal X-ray determinations of **2** and 1,1′-(propane-1,3-diyl)ferrocenium $(TCNQ)_2$ [4] in which the value of Fe–C_2 distance is shorter than that of Fe–C_3. From the NMR data of **4**, we can conclude that the cation of **4** has almost parallel geometry. According to our crystallographic studies of **6**, the Cp protons at 39.77 and 24 ppm can be assigned to $C_{3,4,3',4'}$–H and $C_{2,5,2',5'}$–H, respectively. Finally, it is interesting to find a correlation between α-CH_2 or β-CH_2 protons and the length of interannular bridges. The shifts of α-CH_2 and β-CH_2 protons shift downfield with increasing length of bridge. We believe that this is associated with the structural characteristics of **2**, **4**, and **6**. The value of Fe–C_1 distance will be increased with increasing length of bridge. In this situation, the positive spin density in α-CH_2 protons is decreased as the length of bridge is increased. Consequently, the α-CH_2 and β-CH_2 protons will shift downfield.

Electron paramagnetic resonance

Prins [29] reported the approximate g values for a mononuclear ferrocenium cation to be

$$g_{\parallel} = 2 + 4kx/(1 + x^2)^{1/2}$$

$$g_{\perp} = 2/(1 + x^2)^{1/2}$$

$$k = 1/2 < e_2 \,|\, l_z \,|\, e_2 > \text{ and } x = -\zeta/\delta.$$

In these equations, k is the orbital-reduction factor, ζ is the spin–orbital coupling constant, and δ is a one-electron splitting parameter gauging the effects of crystal fields lower in symmetry than D_5. The parameters k and x contain information on the degree of delocalization of the unpaired electron and on the strength of the low-symmetry perturbation, respectively. An energy-diagram of $^2E_{2g}$ ground-state configuration of ferrocenium is shown in Fig. 8. For a monoferrocenium cation if there is no low-symmetry crystal field ($\delta = 0$) and k is equal to 1, then $g_{\parallel} = 6$ and $g_{\perp} = 0$. As the low-symmetry crystal field distortion increases, both $g_{\parallel}$ and $g_{\perp}$ approach a value of 2. The influence of substituents on the EPR signals for a number of ferrocenium cations has been reported [30]. It is reported [30] that the PF_6^- and $Cl_3CCO_2^-$ salts of 1,1′-(propane,1,3-diyl)ferrocenium cation as polycrys-

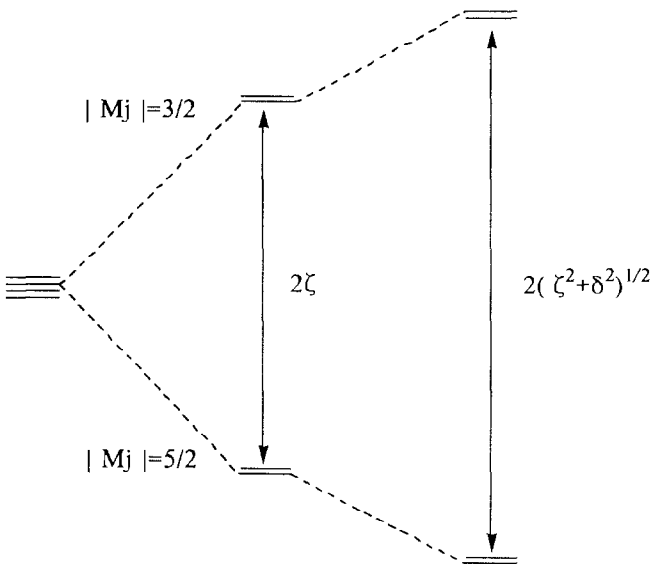

Fig. 8. Energy-level diagram of the $^2E_{2g}$ ground-state configuration of ferrocenium cation.

talline solids give signals with ($g_{\parallel} = 3.86$ and $g_{\perp} = 1.81$) and ($g_{\parallel} = 3.83$ and $g_{\perp} = 1.64$), respectively, at 12 K.

We can now investigate how lowering the symmetry affects the EPR properties. From Table 7, we can conclude that the dipole–dipole interaction in the solid state of **2**–**7** is quite large. Owing to the dipole–dipole interaction, the EPR spectra of the triiodide salts **4** and **6** cannot be observed at 77 K. In the case of **2**, only a broad signal can be seen ($g = 2.00$) at 77 K. It is clear that the dipole–dipole interaction can be somewhat decreased by replacing the counterion from the linear I_3^- to the bulky PF_6^-. Therefore, it is easier to observe the EPR spectra for compounds **3**, **5**, and **7**. Compound **3** shows an EPR signal ($g \simeq 2.00$) at both 300 and 77 K. The axial type EPR spectra can even be seen for compounds **5** and **7**. In the case of **7**, the 77 K EPR spectrum shows $g_{\parallel} = 3.35$ and $g_{\perp} = 1.96$. To eliminate the dipole–dipole interaction and to calculate the low-symmetry parameter as reported by Prins, the unoxidized ferrocene was dissolved in H_2SO_4, the solution frozen at 77 K and the EPR spectra run. These 77 K EPR spectra are just what one would expect for axially symmetric molecules dissolved in a glass. The values of k and x calculated from the observed $g_{\parallel}$ and $g_{\perp}$ values with the aid of the equations given above are presented in Table 7. The k value of 1,1′-(pentane-1,5-diyl)ferrocenium cation indicates that the e_{2g} molecular orbital is essentially localized on the iron atom. The k value of 1,1′-(propane-1,3-diyl) is somewhat lower than the corresponding value for the other. In other words, there is an increased ($d_{x^2-y^2}$, d_{xy})-ring overlap as the rings tilt. The x value of 1,1′-(pentane-1,5-diyl)ferrocenium cation also indicates

that the pentane-1,5-diyl bridge has the most significant low-symmetry perturbation. The evidence that the low-symmetry crystal field contributed from tilted rings and interannular bridge has an important impact on the EPR spectra is available from the room temperature EPR spectrum. Theory and experiment have shown that the fast relaxation times in ferrocenium cations make it difficult to observe EPR signals at high temperatures [29,31]. In general, EPR signals for mononuclear ferrocenium salts are visible at low temperatures but cannot be seen at temperatures above 77 K. However, in compounds **3** and **5** EPR signals can readily be seen at room temperature. To our knowledge, compounds **3** and **5** are the first compounds to show EPR signals at room temperature. We believe that the splitting of e_{2g} orbitals could be the origin of the EPR signals which can be seen at room temperature.

^{57}Fe Mössbauer characteristics

The electronic ground state for a ferrocenium cation can be determined by the Mössbauer technique. It has been reported that the ferrocenyl groups give spectra characterized by large quadrupole splittings (ΔE_Q) in the range of 2.0–2.5 mm/s, while the spectra of ferrocenium cations are characterized by a small or vanishing ΔE_Q, which is mainly due to the decrease in $d_{x^2-y^2}$ and d_{xy} (e_{2g}) population, associated with the removal of one electron from ferrocene. Our Mössbauer studies on bridged ferrocenium salts are consistent with this bonding arrangement. From Table 8, the ΔE_Q values of **6** and **7** are greatly increased. In other words, the interannular pentamethenyl bridges play a rather important role in determining the strength of the low-symmetry crystal field. This is also consistent with the EPR results. As the low-symmetry crystal field distortion increases, the probability of unpaired electron density on the a_{1g} (d_{z^2}) is increased. This results in an increase in ΔE_Q. Since the trends of ΔE_Q and low-symmetry parameter x follow the length of bridges, the interaction of the iron electron with the carbons and protons of the bridges must not be considered to be negligible.

Conclusions

From our NMR studies, the metal–ring distance is the most sensitive factor in determining the electronic delocalization. Furthermore, the electronic ground state for each ferrocenophanium cation is $^2E_{2g}$. The k value of 1,1′-(propane-1,3-diyl)ferrocenium cation indicates that there is an increase of metal–ring overlap as the rings tilt. The splitting of e_{2g} orbitals results in an increase of ΔE_Q and a slower electronic relaxation time.

Acknowledgment

We are grateful for support from the ROC National Science Council.

Supplementary material available. Tables of thermal parameters (1 page) and structure factors (13 pages) of **2** and tables of thermal parameters (2 pages) and structure factors (17 pages) are available from the authors.

References

1 T.-Y. Dong and C.Y. Chou, J. Chem. Soc., Chem. Commun., (1990) 1332.
2 A.G. Nagy, J. Organomet. Chem., 270 (1984) 327.

3 M. Watanabe, K. Sato, I. Motoyama and H. Sano, Chem. Lett., (1983) 1775.
4 C. Willi, A.H. Jr. Reis, E. Gebert and J.S. Miller, Inorg. Chem., 20 (1981) 313.
5 T.H. Barr and W.E. Watts, Tetrahedron, 24 (1968) 6111.
6 M. Hillman and A.G. Nagy, J. Organomet. Chem., 184 (1980) 433.
7 A.G. Nagy and M. Hillman, J. Organomet. Chem., 117 (1976) 55.
8 M. Hillman, B. Gordon, A.J. Weiss and A.P. Guzikowski, J. Organomet. Chem., 155 (1978) 77.
9 E. Fujita, B. Gordon, M. Hillman and A.G. Nagy, J. Organomet. Chem., 218 (1981) 105.
10 J.E. Gordon, H.L. Lentznee and W.E. Watts, Tetrahedron, 27 (1971) 4353.
11 R.M.G. Roberts and J. Silver, J. Organomet. Chem., 263 (1984) 235.
12 T.H. Barr and W.E. Watts, J. Organomet. Chem., 15 (1968) 177.
13 G. Wilkinson, F.G.A. Stone and E.W. Abel (Eds.), Comprehensive Organometallic Chemistry, Vol. 4, Pergamon, Oxford, 1982, p. 487.
14 B.W. Rockett and G. Marr, J. Organomet. Chem., 257 (1983) 209.
15 T.D. Turbitt and W.E. Watts, J. Organomet. Chem., 46 (1972) 107.
16 A.D. Jr. Brown and J.A. Winstead, J. Org. Chem., 36 (1971) 2832.
17 T.H. Barr and W.E. Watts, Tetrahedron, 24 (1968) 3219.
18 J.F. Lee, M.D. Lee and P.K. Tseng, Chemistry (in Chinese), 45 (1987) 50.
19 P. Seiler and J.D. Dunitz, Acta Crystallogr., Sect. B, 35 (1979) 1068.
20 N.J. Mammano, A. Zalkin, A. Landers and A.L. Rheingold, Inorg. Chem., 16 (1977) 297.
21 J. Runsink, S. Swen-Walstra, and T. Migchelsen, Acta Crystallogr., Sect. B, 28 (1972) 1331.
22 A.I. Kitaigorodskii, T.L. Khotsyanova and Y.T. Struchkov, Zh. Fiz. Khim., 27 (1953) 780.
23 C.J. Ballhausen and J.P. Dahl, Acta Chem. Scand., 15 (1961) 1333.
24 J.W. Lauher and R. Hoffmann, J. Am. Chem. Soc., 98 (1976) 1729.
25 D.N. Hendrickson, Y.S. Sohn and H.B. Gray, Inorg. Chem., 10 (1971) 1559.
26 A. Horsfield and A. Wassermann, J. Chem. Soc. (A), (1970) 3202.
27 R. Prins and A. Kortbeek, J. Organomet. Chem., 33 (1971) C33.
28 A. Horsfield and A. Wassermann, J. Chem. Soc., (A), (1972) 187.
29 R. Prins, Mol. Phys., 19 (1970) 603.
30 D.M. Duggan and D.N. Hendrickson, Inorg. Chem., 14 (1975) 955.
31 S.E. Anderson and R. Rai, Chem. Phys., 2 (1973) 216.
32 T. Kurbanov, Kh. Azerb. Khim. Zh., 6 (1981) 104.
33 M.F. Retting and R.S. Drago, J. Am. Chem. Soc., (1969) 1361.
34 J. Happe and R.L. Ward, J. Chem. Phys., 39 (1963) 1211
35 R.J. Fitzgerald and R.S. Drago, J. Am. Chem. Soc., 90 (1968) 2523.